Physica C 468 (2008) 2313–2316

Contents lists available at ScienceDirect

Physica C

journal homepage: www.elsevier.com/locate/physc

Structural and flux-pinning properties of laser ablated $YBa_2Cu_3O_{7-\delta}$ thin films: Effects of self-assembled CeO_2 nanodots on $LaAlO_3$ substrates

Talisha Haywood [a], Sang Ho Oh [b,c], Abebe Kebede [b], Devdas M. Pai [b], Jag Sankar [b], David K. Christen [c], Stephen J. Pennycook [c], Dhananjay Kumar [b,c,*]

[a] Department of Physics, North Carolina A&T State University, Greensboro, NC 27411, United States
[b] Department of Mechanical and Chemical Engineering, North Carolina A&T State University, Greensboro, NC 27411, United States
[c] Materials Science and Technology Division, Oak Ridge National Laboratory, Oak Ridge, TN 37831, United States

ARTICLE INFO

Article history:
Received 11 April 2008
Received in revised form 19 June 2008
Accepted 15 July 2008
Available online 29 August 2008

Keywords:
Nanodots
Critical current density
Pulsed laser deposition

ABSTRACT

Self-assembled nanodots of CeO_2 on (1 0 0) $LaAlO_3$ substrates, generated *in situ* by means of a pulsed laser deposition method prior to the deposition of $YBa_2Cu_3O_{7-\delta}$ (YBCO) films, have been used to modify the superconducting properties of resulting YBCO films. Structural characterization has indicated that CeO_2 layers grow via van der Merwe three-dimensional mode and the islands eventually acquire a pancake type of structure with lateral dimension several times larger than vertical dimension. The three-dimensional growth of CeO_2 islands with (1 0 0) preferred orientation is believed to be associated with its surface energy anisotropy. The magnetization versus temperature and magnetization versus field measurements and analysis have suggested that CeO_2 can affect the superconducting properties of YBCO films favorably or adversely depending on the density of CeO_2 nanodots on the substrate surfaces prior to the deposition of YBCO films.

© 2008 Elsevier B.V. All rights reserved.

1. Introduction

The high-temperature superconducting (HTS) $YBa_2Cu_3O_{7-\delta}$ (YBCO) thin films have been the subject of major research efforts because of the widespread technological applications of these films [1,2]. One of the reasons for continued interest in HTS films is their ability to conduct large non-dissipative currents under high magnetic fields. Conceptually, this can be achieved by spatial inhomogeneities in the material [2]. The inhomogeneities serve to prevent motion of the quantized magnetic filaments (supercurrent vortices) that permeate practical superconducting materials in the presence of a magnetic field. In an ideal, defect-free, and isotropic superconducting material these vortices arrange in a two-dimensional hexagonal lattice, with an inter-vortex spacing a_0 that is related to the macroscopic magnetic flux density, B, according to, $B = 2\phi_0/\sqrt{3}a_0^2$, where, $\phi_0 = 2.07 \times 10^{-7}$ Gauss-cm^2 is the magnetic flux quantum carried by each vortex. Any motion of vortices results in energy dissipation. This motion may occur from a Lorentz-like force from an imposed transport current density, J_c, or even from thermal activation that causes a Brownian-like vortex motion, especially in high-temperature superconductors. Therefore, an ideal homogeneous superconductor, free of flux-pinning defects, could carry no loss-free current in the presence of a magnetic field and hence efforts are made to obtain inhomogeneities in HTS materials without compromising the inherent structure of the HTS system.

The inhomogeneities in HTS materials can arise from crystallographic defects such as dislocations, twin planes, etc. However, studies have shown that the majority of naturally occurring growth defects are either not effective enough to suppress thermal fluctuations or the spatial densities are not high enough to stop the vortex mobility by pinning them in order to maintain the necessary levels of high density electrical currents in high magnetic fields [2,3]. Therefore, it is important to improve further the flux-pinning properties of YBCO thin films by introducing defects. Artificially localized defects may be generated either by irradiation with energetic particles or by creating antiphase boundaries produced by miscut substrates. Recent investigations have shown that one of the most promising approaches to enhance critical current density of YBCO in presence of an applied field is to introduce three-dimensional homogeneous defects (secondary phases) in the matrix. These defects with size in the range of few times YBCO's coherence length (~ a few nanometers) have been found to act as a means to cease vortex mobility [4].

In recent years, pulsed laser deposition (PLD) has emerged as a very functional thin film growth technique that has also been lately applied to introduce/generate nanostructures within epitaxial, textured or polycrystalline thin film matrices. The effectiveness of PLD technique to create nanostructures within a thin film matrix

* Corresponding author. Address: Department of Mechanical and Chemical Engineering, North Carolina A&T State University, Greensboro, NC 27411, United States. Tel.: +1 336 256 1151x2242; fax: +1 336 256 1153.
E-mail address: dkumar@ncat.edu (D. Kumar).

0921-4534/$ - see front matter © 2008 Elsevier B.V. All rights reserved.
doi:10.1016/j.physc.2008.07.008

arises essentially from very convenient tuneability of the process parameter to bring about the growth of second phase predominantly via Volmer–Weber growth mode. Indeed, there are a number of reports where PLD has been utilized to incorporate insulating nanoclusters such as Y_2BaCuO_5 [5,6], Y_2O_3 [7,8], CeO_2 [9], and $BaZrO_3$ (BZO) [10] within YBCO thin film matrix to improve J_c by as much as an order of magnitude. In this work, we report additional information the role of nanostructured substrates on the growth and subsequent superconducting properties of YBCO films [11–13]. The nanostructures on the substrates are generated *in situ* by means of depositing CeO_2 islands prior to the deposition of YBCO films.

2. Experimental

Single and multilayer samples were prepared using pulsed laser deposition (PLD). CeO_2 nanodots of different sizes were prepared on $LaAlO_3$ (LAO) substrates by applying different number of laser pulses onto the CeO_2 target (for example, 10 and 30 pulses). Then a 300 nm thick YBCO layer was deposited over the nanodot layer. The experimental conditions for the deposition of YBCO films include: substrate temperature of 780 °C, an oxygen pressure of 200 mTorr, laser energy of 700 mJ, and laser pulse repetition rate of 10 Hz. All the YBCO films were cooled under an oxygen pressure of 500 Torr. The deposition parameters for CeO_2 nanodots were the same as the deposition parameters for YBCO films in terms of substrate temperature, oxygen pressure, and laser energy. X-ray diffraction (XRD) and scanning transmission electron microscopy (STEM) were carried out to investigate the film microstructures as well as to calculate/measure the average size of CeO_2 nanoparticles/nanoislands. The STEM observations were carried out in a VG HB501UX microscope operated at 100 kV equipped with a Nion aberration corrector. High-angle annular dark-field (HAADF) and bright-field (BF) images were recorded simultaneously. The cross-sectional specimens were prepared by using Ar^+-ion milling method for electron transparency.

The superconducting properties of YBCO/CeO_2/LAO samples were measured using a physical property measurement system with vibrating-sample magnetometer (VSM) feature. Magnetization (M) versus temperature (T) measurements in very low field (10 G) were carried out to determine the transition temperature of each sample. The magnetic field (H) dependence of the critical current density, $J_c(H)$, was determined from magnetization versus field hysteresis (M–H) loops at different temperatures using Bean's critical state model. The field was applied perpendicular to the surface plane of the samples during both M–T and M–H measurements.

3. Results and discussion

X-ray diffraction was used to characterize the samples structurally. Fig. 1 shows the XRD patterns obtained from CeO_2/YBCO bilayered structures with CeO_2 nanodots with two different sizes; one corresponding to 10 laser pulses and the other corresponding to 30 laser pulses impingement on CeO_2 targets. These patterns clearly show that the YBCO films are fully textured with a (00l) orientation (i.e. c-axis orientation). The major reflection from CeO_2 corresponds to the (200) plane intensity, which increases with the number of incident laser pulses on CeO_2 target. The diffraction peaks are relatively weak and broad in the XRD patterns. For the 10-pulse sample, the CeO_2 (200) peak was not resolvable, probably due to the small size and low density of CeO_2 islands. Therefore, high-resolution STEM was used to investigate the nature of CeO_2 growth. The cross-sectional STEM observations suggest that CeO_2 grows in a three-dimensional island mode on $LaAlO_3$ substrate (Fig. 2). The islands grown in 10 pulses CeO_2 were separated from

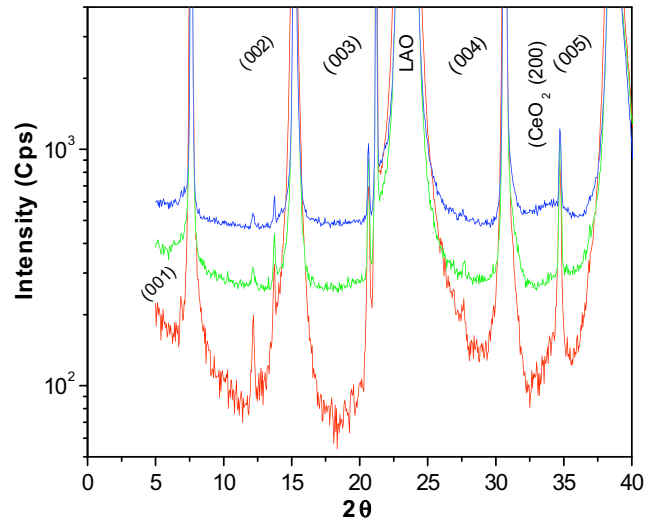

Fig. 1. X-ray diffraction patterns recorded from pure YBCO films (bottom, red) and YBCO films grown on 10 pulses CeO_2 (center, green) and 30 pulses CeO_2 (top, blue) nanodots. (For interpretation of the references to colour in this figure legend, the reader is referred to the web version of this article.)

each other with an average spacing of ~7 nm. Note that in Fig. 2a several islands were projected along the viewing direction as the sample thickness was much larger than the island width/spacing. The island height was measured to be ~1.7 nm in average. The width of each island was varied in a range from 4 nm to 6 nm.

At 10 pulses, most of the CeO_2 islands were separated from each other and were epitaxial on the substrate with an orientation relationship of: $(001)^{[1\bar{1}0]}CeO_2 \| (001)[100]LaAlO_3$. The nominal film thickness of CeO_2 islands was ~1.7 nm. In 30 pulses CeO_2, the islands were coalesced (nominal thickness ~ 4 nm) and this resulted in a rough film surface, as shown in Fig. 2b. The islands were still predominantly oriented with the relationship of $(001)^{[1\bar{1}0]}CeO_2 \| (001)[100]LaAlO_3$. (Let us call this orientation (OR-I).) However, a small fraction of grains in 30 pulses CeO_2 samples possesses a different orientation relationship (OR-II), which is: $(110)^{[1\bar{1}0]}CeO_2 \| (001)[100]LaAlO_3$. (100) islands are relatively flat whereas the small (110) islands are strongly faceted by the inclined {111} planes (Fig. 2b). It often appeared that the (110) islands exist preferentially at the surface steps of $LaAlO_3$ substrate. The presence of periodic misfit dislocations was observed at the interface of (110) islands. The average spacing between misfit dislocations was two and half unit cells of $LaAlO_3$, which could sufficiently relax the misfit strain (+28.5%). In contrast, most of (100) islands showed coherent interfaces with $LaAlO_3$ due to the relatively low misfit strain (−1.3%).

Shown in Fig. 3 are zero-field-cooled (ZFC) M–T plots for the reference YBCO, 10 pulses CeO_2/YBCO, and 30 pulses CeO_2/YBCO samples in an applied field of 10 Oe. These plots resemble a typical M–T plot for type II superconductors. It is clearly seen that while the T_c of all the three sample are almost the same, ~88–89 K, the magnitude of diamagnetic signal from the 10 pulses CeO_2/YBCO sample is highest, which is followed in order by 30 pulses CeO_2/YBCO sample and reference YBCO sample. Indeed, this trend is consistent with the fact that flux-pinning is responsible for the observed diamagnetic level in the applied field of 10 Oe. From a simple estimate of the demagnetization factor $D_z \cong 1 - \frac{2d}{a}$, for a thin film in a perpendicular field (d and a represent the film thickness and lateral dimensions, respectively), it can be seen that the effective field far exceeds the lower critical field, $H_{eff} = H_a\,[1/(1-D_z)] \gg H_{c1}$. With sufficiently strong pinning, however, (e.g., low-field $J_c > 3$ MA/cm^2) the expected field-excluded magnetization is near-Meissner like,

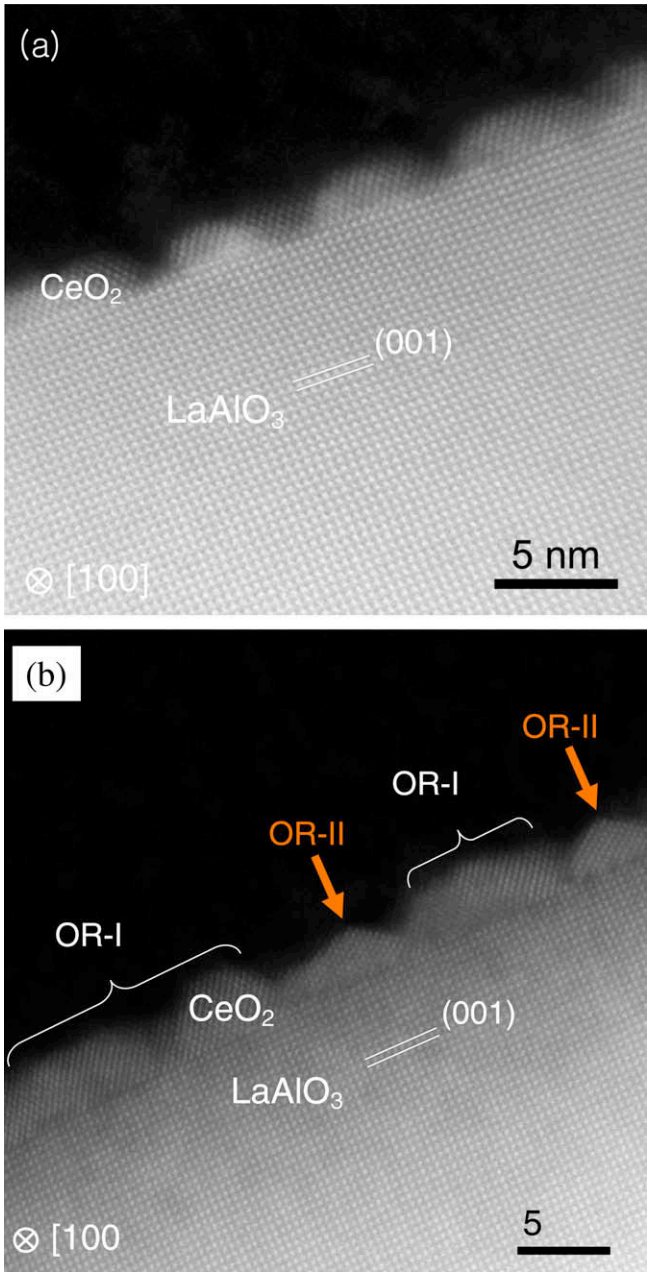

Fig. 2. STEM high-angle annular dark-field images of (a) 10 pulses CeO_2 and (b) 30 pulses CeO_2 on $LaAlO_3$ substrates.

with a saturation value given by $M \cong \frac{a}{12\pi d} H_a$ [14,15]. Evaluation of this expression yields the general magnitude of the observed low-temperature data in Fig. 3 to within the uncertainty in the geometrical factors. Thus, the range of low-field magnetizations probably reflects only some variation in sample-to-sample geometry since the critical current densities of all the materials are quite high, as we now discuss.

Shown in Fig. 4 are the M–H loops recorded from the reference YBCO (a), 10 pulses CeO_2/YBCO (b), and 30 pulses CeO_2/YBCO (c) samples at different temperatures. The critical current density is obtained using these M–H loops and Bean's Model ($J_c = 30\ \Delta M/a$, where ΔM is the hysteresis loop vertical width and a is the average sample size). Fig. 5 compares the temperature dependence of J_c for all three samples, taken in fixed fields of 3 T and 5 T. These field values were chosen for their relevance to potential applications of high-T_c wire in rotating power equipment (motors, generators).

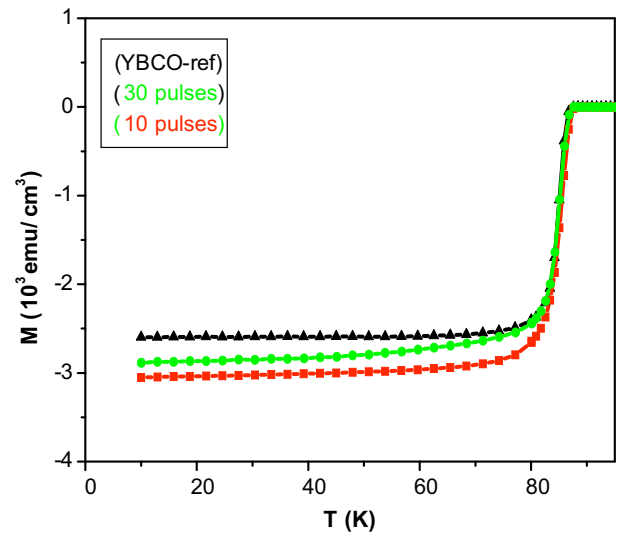

Fig. 3. M–T curves for the reference YBCO and 10 pulses CeO_2/YBCO, and 30 pulses CeO_2/YBCO samples, taken in an applied field of 10 Oe after having been cooled in zero field.

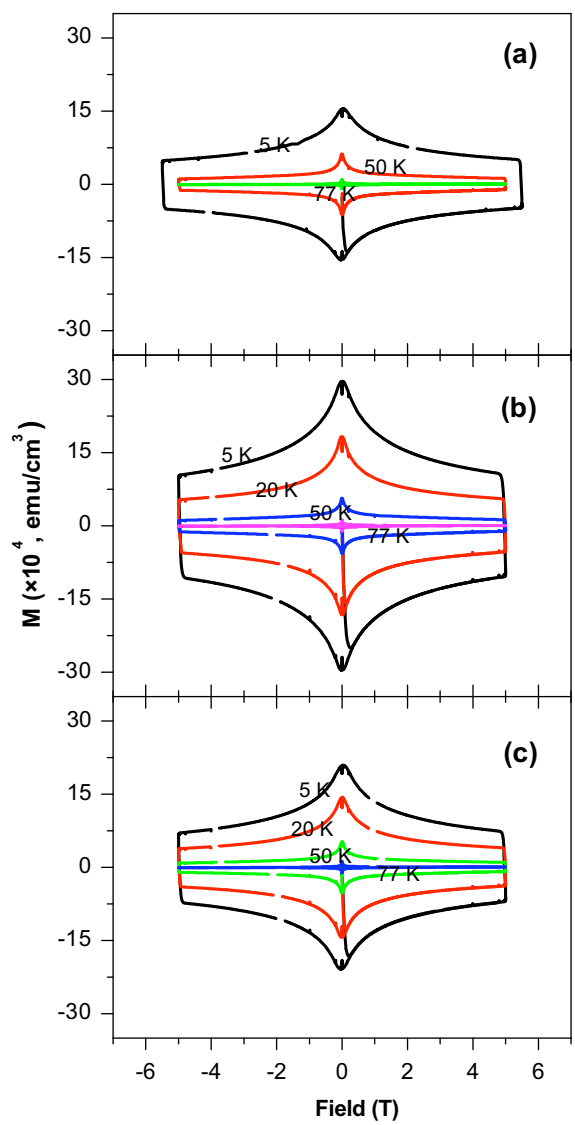

Fig. 4. M–H loops for (a) reference YBCO, (b) 10 pulses CeO_2/YBCO, and (c) 30 pulses CeO_2/YBCO samples recorded at different temperatures.

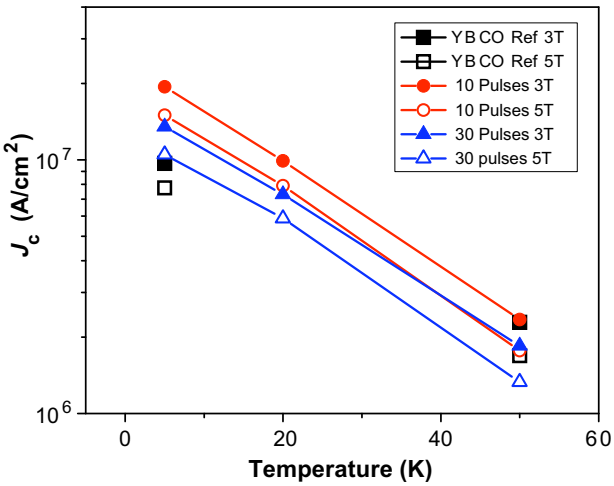

Fig. 5. J_c as a function of temperature at 3 and 5 T for the reference, 10 pulses CeO_2/YBCO and 30 pulses CeO_2/YBCO samples.

Compared to the control sample, the data at low temperatures exhibit improvements in J_c for YBCO deposited on the nanoparticle treated substrates. The substrates with 10 pulses of CeO_2 appear to yield better results than those for the higher pulse number, 30, where for the latter the TEM revealed some coalescence of particles. Recent work has shown that such nanoparticle-decorated substrate surfaces can spawn various types of growth defects in PLD YBCO films deposited upon them [13], and these antiphase boundaries, dislocations, buckled lattice planes, and second-phase precipitates can act as effective pinning sites for improved J_c. As noted above, for the 10-pulse sample, the TEM cross-section observed surface particle spacing of 7 nm is a projection, and does not account for the TEM specimen thickness. We may estimate an actual spacing of from 15 nm to 25 nm. If each particle produced a YBCO defect, then the approximate matching density of pinned vortices would correspond to fields of 3–9 T. Such particle-induced defects could explain the observed enhanced J_c values of Fig. 5. The large density and size of the CeO_2 particles from the 30-pulse deposition also provide improvements compared to the control sample, but the increased surface fraction is not as optimal as that of the 10-pulse sample, at least not at the fields that are experimentally accessible (it is possible that improved flux-pinning might be obtained by the 30-pulse sample at higher vortex density). At 50 K, where thermally activated depinning effects are becoming more important, the decorated substrates yield very little improvement. In fact, the reference sample exhibits in-field J_c that essentially match those of the 10-pulse sample, and exceeds those of the 30-pulse sample. This effect cannot be ascribed to a simple temperature dependence (proximity to T_c), since the measured T_c values of all three samples were nearly identical. Better understanding and full optimization of the effect would come from further studies, where control of both the density and size of CeO_2 nanoparticles, and their effects on the superconductive properties should be explored.

4. Conclusion

The role of surface modification of single crystal substrates via the formation of self-assembled nanodots on the growth and subsequent superconducting properties of $YBa_2Cu_3O_{7-\delta}$ (YBCO) films has been examined. According to the cross-sectional STEM results, CeO_2 grows in a three-dimensional island mode on $LaAlO_3$ substrate surfaces, the size and spacing of which could be controlled by number of incident laser pulses on CeO_2 target. For two different surface particle densities, YBCO films were deposited by PLD and the critical state superconducting properties measurements by vibrating-sample magnetometry. The results show a significant increase in the low-temperature J_c at flux densities that are important for potential applications of superconducting wire. The best results were obtained for an intermediate density of CeO_2 nanoparticles, as determined by high-resolution STEM. The present results point to the need for further work to optimize the size and density of nanoparticles on substrate surfaces for the production of growth-induced strong flux-pinning defects in the deposited superconducting film.

Acknowledgements

This work was supported by a NSF-NIRT Grant DMR-0403480 and by the Center for Advanced Materials and Smart Structures.

References

[1] B. Dam et al., Nature 399 (1999) 439.
[2] D. Larbalestier, A. Gurevich, D.M. Feldmann, A. Ployanskii, Nature 414 (2001) 368.
[3] J.M. Huijbregtse, F.C. Klaassen, A. Szepielow, J.H. Rector, B. Dam, J.Th.M. de Hosson, Supercond. Sci. Technol. 15 (2002) 395.
[4] J. Talvacchio, IEEE Trans. Compon., Hybrids, Manuf. Technol. 12 (1989) 21.
[5] T.J. Haugan, P.N. Barnes, I. Maartense, C.B. Cobb, E.J. Lee, M. Sumption, J. Matter. Res. 18 (2003) 2618.
[6] T.J. Haugan, P.N. Barnes, R. Wheeler, F. Meisenkothen, M. Sumption, Nature (London) 430 (2004) 867.
[7] A.A. Gapud, D. Kumar, S.K. Viswanathan, C. Cantoni, M. Varela, J. Abiade, S.J. Pennycook, D.K. Christen, Supercond. Sci. Technol. 18 (2005) 1502.
[8] T.A. Campbell, T.J. Haugen, I. Maartense, J. Murphy, L. Brunke, P.N. Branes, Physica C 423 (2005) 1.
[9] P.N. Barnes, T.J. Haugen, C.V. Varanasi, T.A. Campbell, Appl. Phys. Lett. 85 (2004) 18.
[10] A. Goyal, S. Kang, K.J. Leonard, P.M. Martin, A.A. Gapud, M. Verala, M. Paranthaman, A.O. Ijaduola, J.R. Thompson, D.K. Christen, S.J. Pennycook, Supercond. Sci. Technol. 18 (2005) 1533.
[11] A. Crisan, S. Fujiwara, J.C. Nie, A. Sundaresan, H. Ihara, Appl. Phys. Lett. 79 (2001) 4547.
[12] K. Matsumoto, T. Horide, A. Ichinose, S. Horii, Y. Yoshida, M. Mukaida, Jpn. J. Appl. Phys. 44 (2005) L246. Part 2.
[13] T. Aytug, M. Paranthaman, K.J. Leonard, S. Kang, P.M. Martin, L. Heatherly, A. Goyal, A.O. Ijaduola, J.R. Thompson, D.K. Christen, Phys. Rev. B 74 (2006) 184505.
[14] John R. Clem, Alvaro Sanchez, Phys. Rev. B 50 (1994) 9355.
[15] Th. Herzog, H.A. Radovan, P. Ziemann, E.H. Brandt, Phys. Rev. B 56 (1997) 2871.